Transmission and Attenuation of the Dominant Mode in Uniformly Bent Circular Hollow Waveguides for the Infrared: Scalar Analysis

Shin-ichi Abe and Mitsunobu Miyagi, *Senior Member, IEEE*

Abstract—**We numerically evaluate electric field distributions, phase constants, and attenuation constants of the lowest eigenmode in the general class of uniformly bent circular hollow waveguides. The analysis is based on a scalar equation, and numerical results are compared with those of existing approximate theories. Numerically fitting curves of attenuation constants are also presented.**

I. Introduction

INFRARED lasers such as CO and CO_2 lasers have been widely used in industry and medicine. Hollow waveguides are potential guiding media for delivering high-powered laser lights [1]. In the hollow waveguides which support leaky modes or generalized surface wave modes [2], power losses always exist even when the waveguides are straight, for outer claddings do not function as totally reflecting media [3]. In overmoded straight slab or circular hollow waveguides, power losses have been fully analyzed by using the concept of surface impedance or admittance defined at the boundary between a hollow core and one of reflecting media [4], [5]. Several possible methods to reduce straight waveguide losses have been proposed [4], [6]. When waveguides are bent, losses increase additionally. Therefore, in hollow waveguides it is very important to evaluate power losses caused by a bend.

In uniformly bent overmoded slab hollow waveguides, bending losses have been analyzed based on a scalar equation deduced from Maxwell's equations [7], [8]. Expressions of attenuation constants for lower order modes have been explicitly presented [8]. For bent circular waveguides, several methods have been used to predict bending losses; these are based on ray analysis [9], mode coupling analysis [10], or Maxwell's equations [11], [12]. For a large bending radius, Marcatili and Schmeltzer [11] derived expressions for attenuation constants in a metallic and dielectric waveguides. However, their analyses were not rigorous and exact analyses were made in [12] for the general class of circular hollow waveguides including a metallic or dielectric waveguide. Wilson *et al.* [13] compared the experimental results with those predicted in [11] and [12]. They also analyzed nonuniformly bent waveguides. For sharply bent waveguides, where the electric fields are concentrated near the outer edge of the waveguides, losses of a linearly polarized mode whose polarization is parallel to the bending plane were discussed in [14], where the attenuation constant was shown to be proportional to the curvature with a proportional constant of a normalized surface admittance or the real part of the complex refractive index of metal. A special case where a normalized surface admittance is equal to a normalized surface impedance was also discussed [14], and it was also shown that losses are proportional to the curvature. However, in these two cases and in cases reported elsewhere, the analysis was essentially based on a slab geometry, and the diameter of the hollow core was not taken into account; i.e., coupling effects between parallel and perpendicular polarizations to the waveguide wall were completely neglected. In order to take the coupling effect into account, a rather intuitive analysis was made in [15] based on a scalar analysis. As the coupling effect was introduced by the parameter b including a bending radius and core radius, the attenuation constants of modes whose polarizations are parallel or perpendicular to the bending plane are no longer proportional to the curvature. However, as the analysis itself is rather intuitive, the results should be checked numerically by using a rigorous analysis. Furthermore, the limits of mild bending and strong bending are not evaluated numerically because exact results have not yet been established.

In this paper, we present numerical results of field distributions, phase constants, and bending losses of the lowest eigenmode in uniformly bent circular hollow waveguides with arbitrary bending radii. The lowest eigenmode with linear polarization corresponds to the EH_{11} modes in Marcatili and Schmeltzer's nomenclature [11] or to the HE_{11} modes in the nomenclature of [12], which is generally employed in fiber waveguides. The analysis is based on a scalar wave equation. We clarify the limits of the theories [12], [15] derived previously. Numerically fitting curves are also presented for the attenuation constants of the lowest eigenmode in the general class of overmoded circular hollow waveguides.

Manuscript received November 14, 1989; revised August 14, 1990. This work was supported by a Scientific Research Grant-in-Aid (63850072) from the Ministry of Education, Science, and Culture of Japan.

The authors are with the Department of Electrical Communications, Faculty of Engineering, Tohoku University, Sendai, 980 Japan.

IEEE Log Number 9041078.

II. Scalar Equation

We employ the toroidal coordinate system for the analysis of the uniformly bent circular hollow waveguide shown in Fig. 1. Here n_0 is the refractive index in the core region, T is

0018-9480/91/0200-0230$01.00 ©1991 IEEE

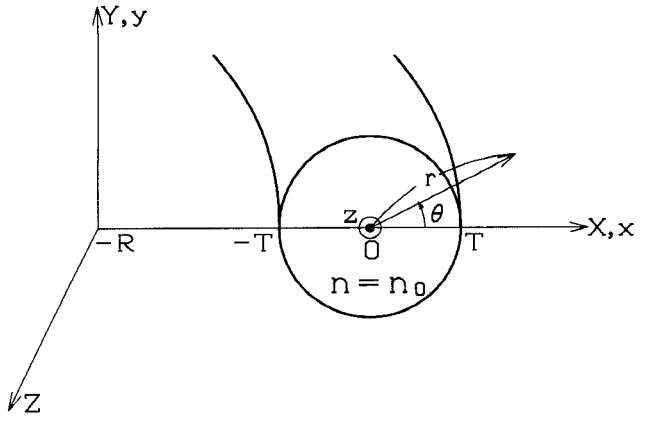

Fig. 1. Toroidal coordinate system for bent circular hollow waveguides.

the core radius, and R is the bending radius. To analyze low-loss waveguides for the transmission of high-powered laser lights, it is assumed that T is sufficiently large compared with the wavelength of transmitted light and that a normalized surface impedance z_{TE} and y_{TM} [12] defined at $r = T$ is sufficiently small compared with those of the hollow core. In addition, it is also assumed that R is sufficiently large compared with the core radius T. Based on these conditions, we analyze linearly polarized modes in the circular hollow waveguides and discuss the electric fields determined from a scalar equation.

Let the axial (z axis) phase constant be β. Then, the transverse electric field component E is determined by the following scalar equation (see Appendix I):

$$\frac{\partial^2 E}{\partial r^2} + \frac{1}{r}\frac{\partial E}{\partial r} + \frac{1}{r^2}\frac{\partial^2 E}{\partial \theta^2} + \left[n_0^2 k_0^2\left(1 + 2\frac{r}{R}\cos\theta\right) - \beta^2\right]E = 0. \tag{1}$$

By solving (1) with appropriate boundary conditions, the attenuation constants can be determined by field distributions in a core region, as described in subsection IV-A.

III. Field Distribution and Phase Constant

A. Formulation

In the core region, the transverse electric field E of the eigenmode of the bent waveguide, which is even-symmetrical around $\theta = 0$, can be expanded as follows [16]:

$$E = \exp(-j\beta z)\sum_{\nu=0}^{\infty}\sum_{p=1}^{\infty} A_{\nu p} J_\nu\left(\frac{\sigma_{\nu p}}{T} r\right)\cos(\nu\theta) \tag{2}$$

where $\sigma_{\nu p}$ is the pth zero of $J\nu(x)$ except for zero and we have assumed that fields are fully confined in the core region. For numerical convergence, basis functions should be carefully chosen [17], [18]. In our analysis, each term of (2) corresponds to an eigenmode in a straight waveguide. The expansion is convenient in evaluating the mode conversion for mild bending.

Substituting (2) into (1) and using the orthogonal relations of Bessel or trigonometric functions, we obtain

$$K_p^\nu A_{\nu p} + \sum_{q=1}^{\infty}\left[Q_{qp}^{\nu-1} A_{\nu-1,q} + Q_{pq}^{\nu} A_{\nu+1,q}\right] = 0 \qquad (\nu = 0,1,\cdots;\ p = 1,2,\cdots) \tag{3}$$

where K_p^ν and Q_{pq}^ν are defined by

$$K_p^\nu = \left(u^2 - \sigma_{\nu p}^2\right)(1+\delta_{\nu 0})J_\nu'^2(\sigma_{\nu p}) \tag{4}$$

$$Q_{pq}^\nu = 2b(1+\delta_{\nu 0})\int_0^1 r^2 J_\nu(\sigma_{\nu p} r) J_{\nu+1}(\sigma_{\nu+1,q} r)\, dr \tag{5}$$

$$\delta_{\nu 0} = \begin{cases} 1 & \nu = 0 \\ 0 & \nu \neq 0 \end{cases} \tag{6}$$

and the normalized phase constant u and the parameter b related to curvature are defined by

$$u^2 = \left(n_0^2 k_0^2 - \beta^2\right)T^2 \tag{7}$$

$$b = (n_0 k_0 T)^2 T/R. \tag{8}$$

It should be noted that the normalized transverse phase constant u and expansion coefficients $A_{\nu p}$ are a function only of b. Equation (3) can be transformed to the matrix equation as follows:

$$\mathbb{M}\mathbb{B} = u^2\mathbb{B} \tag{9}$$

where the symmetric matrix $\mathbb{M}$ is represented by

$$\mathbb{M} = \begin{bmatrix} \mathbb{L}^{(0)} & \mathbb{N}^{(0)} & 0 & \cdots & 0 \\ {}^t\mathbb{N}^{(0)} & \mathbb{L}^{(1)} & \mathbb{N}^{(1)} & \ddots & \vdots \\ 0 & {}^t\mathbb{N}^{(1)} & \mathbb{L}^{(2)} & \mathbb{N}^{(2)} & \ddots \\ \vdots & \ddots & {}^t\mathbb{N}^{(2)} & \mathbb{L}^{(3)} & \ddots \\ 0 & & \ddots & \ddots & \end{bmatrix}. \tag{10}$$

${}^t\mathbb{N}^{(\nu)}$ is the transposed matrix of $\mathbb{N}^{(\nu)}$, and elements $L_{pq}^{(\nu)}$ and $N_{pq}^{(\nu)}$ of partial matrices $\mathbb{L}^{(\nu)}$ and $\mathbb{N}^{(\nu)}$ are represented by

$$L_{pq}^{(\nu)} = \sigma_{\nu p}^2 \delta_{pq} \tag{11}$$

$$N_{pq}^{(\nu)} = -\frac{Q_{pq}^\nu}{(1+\delta_{\nu 0})^{1/2} J_\nu'(\sigma_{\nu p}) J_{\nu+1}'(\sigma_{\nu+1,q})}. \tag{12}$$

The vector $\mathbb{B}$ in (9) is defined by

$$\mathbb{B} = \begin{bmatrix} \mathbb{B}^{(0)} \\ \mathbb{B}^{(1)} \\ \mathbb{B}^{(2)} \\ \mathbb{B}^{(3)} \\ \mathbb{B}^{(4)} \\ \vdots \end{bmatrix} \tag{13}$$

whose partial vector $\mathbb{B}^{(\nu)}$ is related to the expansion coefficients $A_{\nu p}$ as

$$\mathbb{B}^{(\nu)} = (1+\delta_{\nu 0})^{1/2}\begin{bmatrix} J_\nu'(\sigma_{\nu 1})A_{\nu 1} \\ J_\nu'(\sigma_{\nu 2})A_{\nu 2} \\ J_\nu'(\sigma_{\nu 3})A_{\nu 3} \\ J_\nu'(\sigma_{\nu 4})A_{\nu 4} \\ J_\nu'(\sigma_{\nu 5})A_{\nu 5} \\ \vdots \end{bmatrix}. \tag{14}$$

Equation (9) means that the square of normalized transverse phase constants u^2 and expansion coefficients $A_{\nu p}$ can be determined as eigenvalues and eigenvectors of the symmetric matrix $\mathbb{M}$, respectively.

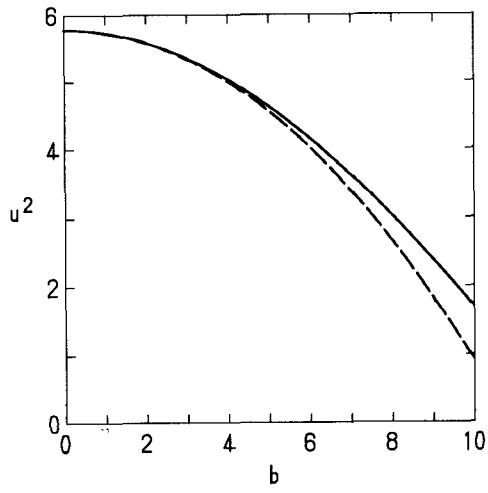

Fig. 2. u^2 of the lowest eigenmode in gently bent hollow waveguides. The solid line corresponds to the numerical analysis. The dashed line corresponds to the perturbation theory [12].

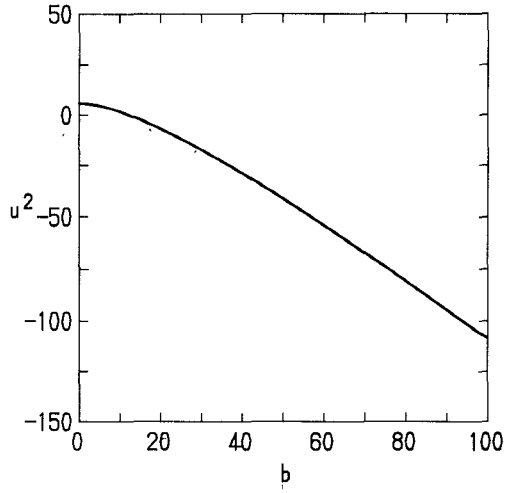

Fig. 3. u^2 of the lowest eigenmode in hollow waveguides.

B. Normalized Transverse Phase Constant and Electric Field Distribution of Dominant Mode

The eigenvalues and eigenvectors of (9) are numerically solved by Jacobi's method. How the expansion is made in (2) and how the matrix size of $\mathbb{M}$ is chosen are described in detail in Appendix II. Fig. 2 shows u^2 of the lowest eigenmode in the gently bent waveguides. The solid line corresponds to the numerical result. The dashed line corresponds to u^2 of the HE_{11} mode predicted by the perturbation theory of vector equations [12], which leads to

$$u^2 = \sigma_{01}^2 - \frac{1}{6}\frac{b^2}{\sigma_{01}^2}\left(1+\frac{4}{\sigma_{01}^2}\right). \tag{15}$$

It should be noted that the perturbation theory evaluates u^2 very precisely when b is smaller than 4. The quantity u^2 for the sharply bent waveguides as well as the gently bent waveguides is also shown in Fig. 3. The value of u^2 decreases; i.e., the axial phase constant β increases due to bending and becomes negative when b is large. This is because the electric field of the dominant mode is concentrated in the region where the refractive index is effectively higher than n_0.

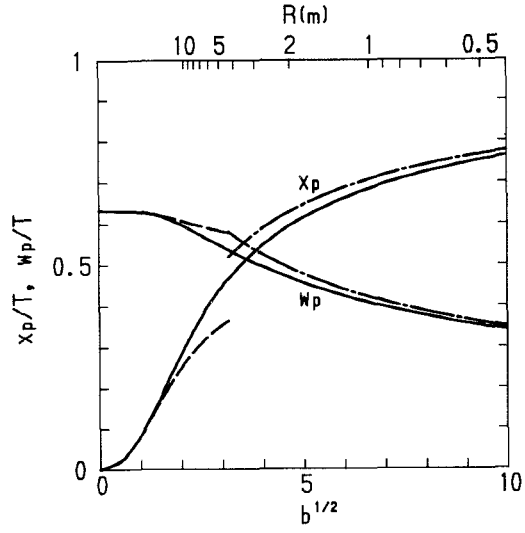

Fig. 4. x_p and w_p in bent hollow waveguides. Solid lines correspond to the numerical analysis. Dashed lines correspond to the perturbation theory [12]. Dot-dash lines are calculated by Marhic's theory [19]. The upper scale corresponds to the bending radius R for $n_0 = 1$, $T = 0.5$ mm, and $\lambda = 10.6$ μm.

The electric field distribution is determined from expansion coefficients A_{vp}. In order to see field deformations caused by bending, we evaluate the position, x_p, where the amplitude of field becomes maximum in the x direction at $y = 0$, and the half width of half maximum, w_p, in the y direction at $x = x_p$. Fig. 4 shows x_p and w_p of the lowest eigenmode. Solid lines correspond to the present theory; dashed lines correspond to the perturbation theory [12] (see Appendix III). It can be seen that the perturbation theory can predict x_p and w_p very precisely when b is smaller than 4. Dotted dashed lines correspond to Marhic's theory [19] (see Appendix III). His theory can well predict x_p and w_p when b becomes large.

IV. Attenuation Constant

A. Formulation

Attenuation constants α of modes are determined by the ratio of the radiated power from a hollow core to a cladding to the transmitted power in a core region as follows [20]:

$$2\alpha = \frac{\oint_c \mathrm{Re}\left[E_\theta H_z^* - E_z H_\theta^*\right] dc}{\iint_s \mathrm{Re}\left[E_x H_y^* - E_y H_x^*\right] dS} \tag{17}$$

where the integrals in the numerator and the denominator are the line integral around core-cladding boundary and the surface integral in the core region, respectively. We consider here the attenuation constants of modes whose polarization direction is perpendicular or parallel to the bending plane (x-z plane).

For the perpendicular polarization, one can express E_y, E_z, H_x, and H_z of lower order modes as

$$E_y = E \tag{18}$$

$$H_x = j\frac{1}{\omega\mu_0}\left(\frac{\partial E_z}{\partial y} + j\beta E_y\right) \doteqdot -n_0\left(\frac{\epsilon_0}{\mu_0}\right)^{1/2} E \tag{19}$$

$$E_z = -j\frac{1}{\omega n_0^2 \epsilon_0}\left(\frac{\partial H_y}{\partial x} - \frac{\partial H_x}{\partial y}\right) \doteqdot -j\frac{1}{n_0 k_0}\frac{\partial E}{\partial y} \tag{20}$$

$$H_z = j\frac{1}{\omega\mu_0}\left(\frac{\partial E_y}{\partial x} - \frac{\partial E_x}{\partial y}\right) \doteqdot j\frac{1}{\omega\mu_0}\frac{\partial E}{\partial x} \tag{21}$$

where we have assumed [12]

$$E_y \gg E_z \gg E_x = 0 \tag{22}$$

$$H_x \gg H_z \gg H_y = 0. \tag{23}$$

Similarly, for the parallel polarization, we have

$$E_x = E \tag{24}$$

$$H_y \doteqdot n_0\left(\frac{\epsilon_0}{\mu_0}\right)^{1/2} E \tag{25}$$

$$E_z \doteqdot -j\frac{1}{n_0 k_0}\frac{\partial E}{\partial x} \tag{26}$$

$$H_z \doteqdot -j\frac{1}{\omega\mu_0}\frac{\partial E}{\partial y} \tag{27}$$

where we have assumed

$$E_x \gg E_z \gg E_y = 0 \tag{28}$$

$$H_y \gg H_z \gg H_x = 0. \tag{29}$$

On the other hand, tangential components E_θ and H_θ are determined by the boundary conditions [12]:

$$E_\theta = \frac{\omega\mu_0}{n_0 k_0} z_{\mathrm{TE}} H_z \tag{30}$$

$$H_\theta = -\frac{n_0 k_0}{\omega\mu_0} y_{\mathrm{TM}} E_z. \tag{31}$$

Note that (30) and (31) can be used when $n_0 k_0 T \gg 1$. Therefore, E_θ and H_θ in the numerator of (17) are expressed by using $\partial E/\partial x$ and $\partial E/\partial y$ at $r = T$ as

$$E_\theta \doteqdot j\frac{z_{\mathrm{TE}}}{n_0 k_0}\frac{\partial E}{\partial x} \tag{32}$$

$$H_\theta \doteqdot j\frac{y_{\mathrm{TM}}}{\omega\mu_0}\frac{\partial E}{\partial y} \tag{33}$$

for the perpendicular polarization and

$$E_\theta \doteqdot -j\frac{z_{\mathrm{TE}}}{n_0 k_0}\frac{\partial E}{\partial y} \tag{34}$$

$$H_\theta \doteqdot j\frac{y_{\mathrm{TM}}}{\omega\mu_0}\frac{\partial E}{\partial x} \tag{35}$$

for the parallel polarization. By substituting (18)–(35) into (17), one can express attenuation constants $\alpha_\perp$ ($\alpha_\parallel$) of the linearly polarized mode whose polarization is perpendicular (parallel) to the plane of curvature as follows:

$$\alpha_\perp = \frac{\oint_c \left|\frac{\partial E}{\partial x}\right|^2 dc\,\mathrm{Re}(z_{\mathrm{TE}}) + \oint_c \left|\frac{\partial E}{\partial y}\right|^2 dc\,\mathrm{Re}(y_{\mathrm{TM}})}{2n_0^2 k_0^2 \iint_S |E|^2\, dS} \tag{36}$$

$$\alpha_\parallel = \frac{\oint_c \left|\frac{\partial E}{\partial y}\right|^2 dc\,\mathrm{Re}(z_{\mathrm{TE}}) + \oint_c \left|\frac{\partial E}{\partial x}\right|^2 dc\,\mathrm{Re}(y_{\mathrm{TM}})}{2n_0^2 k_0^2 \iint_S |E|^2\, dS}. \tag{37}$$

In order to separate material and structural parameters in the above two equations, we express $\alpha_\perp$ and $\alpha_\parallel$ of the mth order eigenmode whose angular dependence is $\cos(n\theta)$ or $\sin(n\theta)$ in straight waveguides by normalized forms as follows:

$$\frac{\alpha_\perp}{\alpha_{\mathrm{st}}} = g_m\frac{1}{1+f} + g_s\frac{f}{1+f} \tag{38}$$

$$\frac{\alpha_\parallel}{\alpha_{\mathrm{st}}} = g_s\frac{1}{1+f} + g_m\frac{f}{1+f} \tag{39}$$

where α_{st} is the attenuation constant of the eigenmode in straight waveguides [4], defined by

$$\alpha_{\mathrm{st}} = \frac{\sigma_{nm}^2}{2(n_0 k_0 T)^2 T}\mathrm{Re}(z_{\mathrm{TE}} + y_{\mathrm{TM}}) \tag{40}$$

and g_m and g_s are functions of b only and are defined by

$$g_m = \frac{T^3}{\sigma_{nm}^2}\frac{\oint_c \left|\frac{\partial E}{\partial x}\right|^2 dc}{\iint_S |E|^2\, dS} \tag{41}$$

$$g_s = \frac{T^3}{\sigma_{nm}^2}\frac{\oint_c \left|\frac{\partial E}{\partial y}\right|^2 dc}{\iint_S |E|^2\, dS}. \tag{42}$$

The parameter f, defined by

$$f = \mathrm{Re}(y_{\mathrm{TM}})/\mathrm{Re}(z_{\mathrm{TE}}) \tag{43}$$

determines a property of cladding. One can see that the attenuation constants $\alpha_\perp$ and $\alpha_\parallel$ vary between $g_m\alpha_{\mathrm{st}}$ and $g_s\alpha_{\mathrm{st}}$.

B. Numerical Calculations of Attenuation Constants of the Dominant Mode

We first show the normalized attenuation constant $\alpha_\perp/\alpha_{\mathrm{st}}$ of the lowest eigenmode as a function of f in Fig. 5. The curves corresponding to $f = 0$ and ∞ are exactly g_m and g_s,

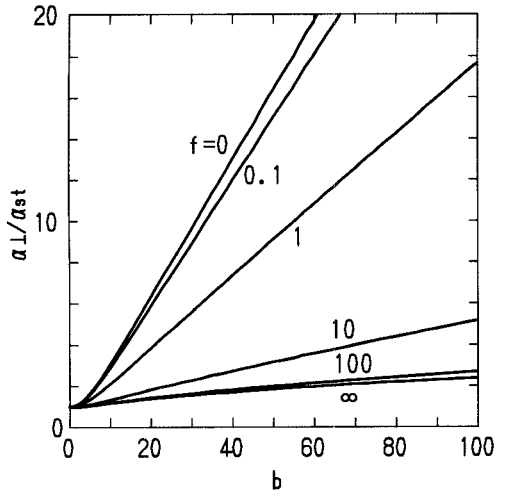

Fig. 5. Normalized attenuation constant $\alpha_\perp/\alpha_{st}$ of the lowest eigenmode in bent hollow waveguides.

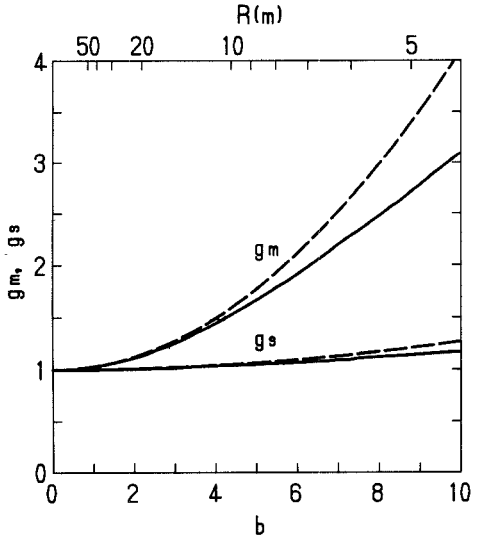

Fig. 6. g_m and g_s for the lowest eigenmode in gently bent hollow waveguides. Solid lines correspond to the numerical analysis. Dashed lines correspond to the perturbation theory, i.e., eqs. (44) and (45). The upper scale corresponds to the bending radius R for $n_0=1$, $T=0.5$ mm, and $\lambda=10.6$ μm.

respectively. In ordinary metallic waveguides at 10.6 μm wavelength, f is of the order of 10^3. On the other hand, in dielectric-coated metallic waveguides f is of the order of 10. As g_m is larger than g_s for the lowest eigenmode, $\alpha_\perp/\alpha_{st}$ decreases and conversely $\alpha_\parallel/\alpha_{st}$ increases when f increases.

Fig. 6 shows g_m and g_s of the lowest eigenmode for the gently bent waveguide. Solid lines correspond to the present theory; dashed lines are calculated by using the perturbation theory [12], where g_m and g_s are expressed by

$$g_m = 1+\frac{1}{3}\frac{b}{\sigma_{01}^2}\left[1+\frac{4}{\sigma_{01}^2}+\frac{3}{8}(\sigma_{01}^2-2)\right] \tag{44}$$

$$g_s = 1+\frac{1}{3}\frac{b}{\sigma_{01}^2}\left[1+\frac{4}{\sigma_{01}^2}-\frac{3}{8}(\sigma_{01}^2-2)\right]. \tag{45}$$

It can be seen that g_m and g_s predicted by the perturbation

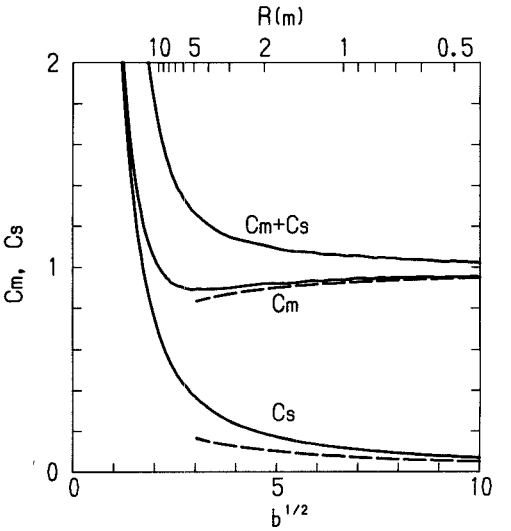

Fig. 7. c_m, c_s, and c_m+c_s for the lowest eigenmode in bent hollow waveguides. Solid lines correspond to the numerical analysis. Dashed lines are results calculated by eqs. (50) and (51). The upper scale corresponds to the bending radius R for $n_0=1$, $\lambda=10.6$ μm, and $T=0.5$ mm.

theory are very close to the numerical values when b is smaller than 4.

In order to obtain more useful explicit formulas for the attenuation constants, we express $\alpha_\perp$ and $\alpha_\parallel$ of (36) and (37) as follows:

$$\alpha_\perp = \frac{1}{R}\left[c_m \mathrm{Re}(z_{TE})+c_s \mathrm{Re}(y_{TM})\right] \equiv c_m\alpha_{TE}+c_s\alpha_{TM} \tag{46}$$

$$\alpha_\parallel = \frac{1}{R}\left[c_s \mathrm{Re}(z_{TE})+c_m \mathrm{Re}(y_{TM})\right] \equiv c_s\alpha_{TE}+c_m\alpha_{TM} \tag{47}$$

where c_m and c_s are parameters depending on only b and are defined by

$$c_m = \frac{T^3}{2b}\frac{\oint_c \left|\frac{\partial E}{\partial x}\right|^2 dc}{\iint_s |E|^2\, dS} \tag{48}$$

$$c_s = \frac{T^3}{2b}\frac{\oint_c \left|\frac{\partial E}{\partial y}\right|^2 dc}{\iint_s |E|^2\, dS}. \tag{49}$$

Equations (46) and (47) mean that attenuation constants $\alpha_\perp$ and $\alpha_\parallel$ in circular waveguides are represented by an appropriate combination of attenuation constants of the TE (α_{TE}) and TM modes (α_{TM}) in sharply bent slab waveguide with suitable weighting parameters depending on b. Although expressions similar to (46) and (47) were given in a previous paper [15] by assuming that $c_m+c_s=1$ and employing a rather intuitive analysis, no assumption has been made in deriving (46) and (47).

Fig. 7 shows the weighting parameters c_m and c_s of the lowest eigenmode, which are simply obtained by multiplying

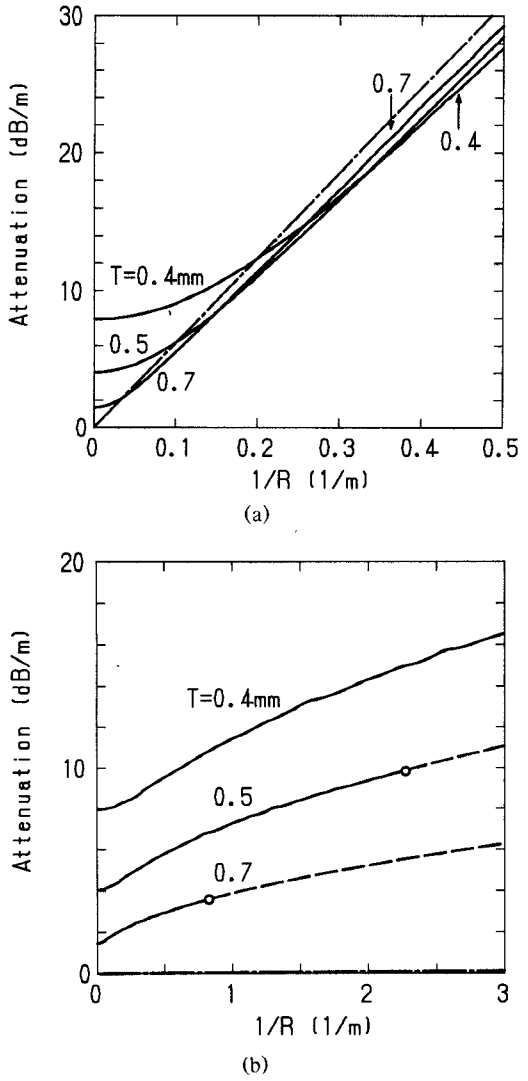

Fig. 8. Attenuation constants (a) $\alpha_{\|}$ and (b) $\alpha_{\perp}$ of the lowest eigenmode in a hollow nickel waveguide at $\lambda = 10.6$ μm. The solid lines correspond to the numerical analysis. The dot–dash curves correspond to (a) α_{TM} and (b) α_{TE}, respectively. The small fluctuations in the curves of (b) are caused by numerical errors arising from the small size of the matrix used. The small circles in the figure correspond to $b = 100$. The dashed curves are drawn by using numerically fitting curves of eqs. (52) and (53).

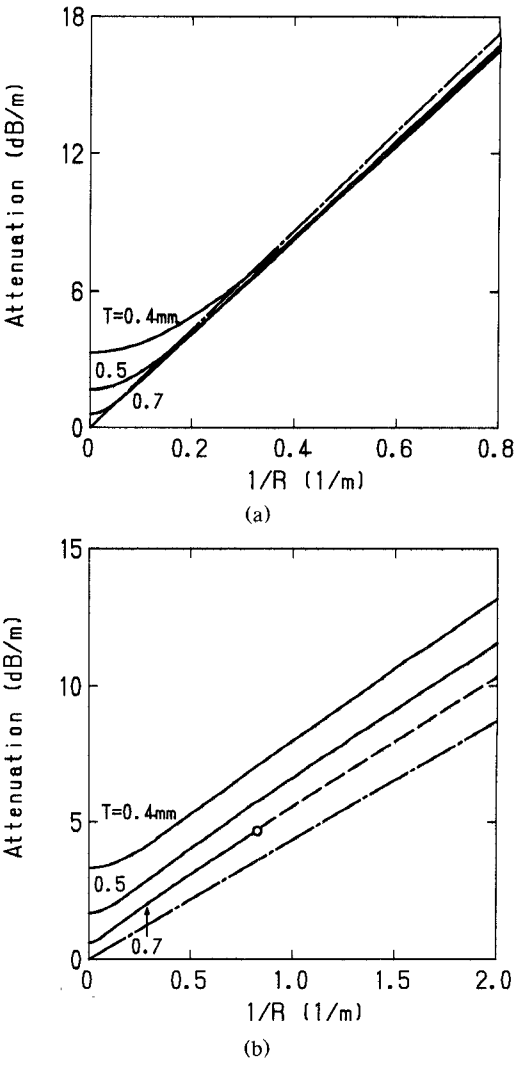

Fig. 9. Attenuation constants (a) $\alpha_{\|}$ and (b) $\alpha_{\perp}$ of the lowest eigenmode in a hollow silica waveguide at $\lambda = 10.6$ μm. The solid lines, the dashed curve, and the small circles have the same meanings as in Fig. 8.

$\sigma_{01}^2/2b$ by g_m and g_s. Solid lines correspond to the present theory; dashed lines correspond to the theory described in the reference [15], which gives

$$c_m = 1 - \frac{1}{2}b^{-1/2} \tag{50}$$

$$c_s = \frac{1}{2}b^{-1/2}. \tag{51}$$

Although the theory in [15] itself is based on a rather intuitive treatment, the agreement of the results can be regarded as sufficient when b becomes large. The smaller the bending radius R, the closer c_m approaches 1 and c_s approaches 0. In other words, the smaller the bending radius R, the closer $\alpha_{\perp}/\alpha_{TE}$ and $\alpha_{\|}/\alpha_{TM}$ approach unity. This is because the circular boundary resembles the straight one for the linearly polarized light as the field distribution becomes concentrated near the outer edge of the waveguide for sufficiently small bending radii. However, this does not simply mean that $\alpha_{\perp}$ or $\alpha_{\|}$ approach α_{TE} or α_{TM}, respectively, which is definitely shown in the examples described below numerically. The ratios of attenuation constants $\alpha_{\perp}/\alpha_{TE}$ and $\alpha_{\|}/\alpha_{TM}$ in a waveguide with a large core rapidly approach unity when bending radii are large.

In order to present explicit expressions for c_m and c_s, the numerical curves are approximated by a method of least square. As a result, we have

$$c_m = 1 - 0.231b^{-1/2} - 1.98b^{-1} + 5.20b^{-3/2} \tag{52}$$

$$c_s = 0.570b^{-1/2} + 1.12b^{-1} + 1.45b^{-3/2} \tag{53}$$

which are not distinguishable from the numerical results in Fig. 7. We also show numerically calculated $c_m + c_s$. One should note that $c_m + c_s$ approaches unity when b becomes large.

Parts (a) and (b) of Fig. 8 show attenuation constants $\alpha_{\|}$ and $\alpha_{\perp}$ in a hollow nickel waveguide ($n_0 = 1$) with various core radii. The wavelength of the light is 10.6 μm and the complex refractive index $n_0(n - j\kappa)$ of nickel is assumed to

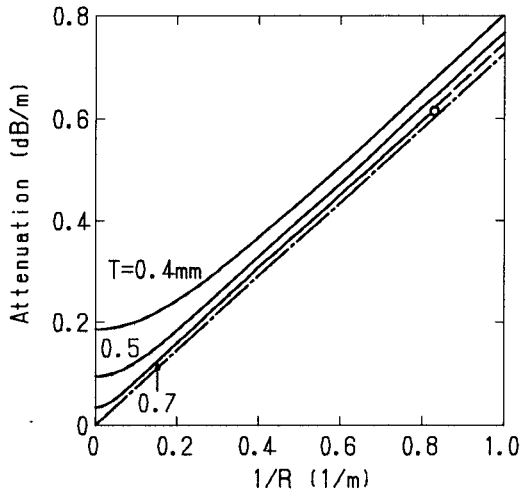

Fig. 10. Attenuation constants $\alpha_{\|}$ and $\alpha_{\perp}$ of the lowest eigenmode in a germanium-coated nickel hollow waveguide at $\lambda = 10.6\ \mu$m. The solid lines, the dashed line, and the small circles have the same meanings as in Fig. 8. The dot–dash curve corresponds to $\alpha_{TE} = \alpha_{TM}$.

be $7.11 - j38.3$ [4], where

$$z_{TE} = \left[(n - j\kappa)^2 - 1\right]^{-1/2} \tag{54}$$

$$y_{TM} = \frac{(n - j\kappa)^2}{\left[(n - j\kappa)^2 - 1\right]^{1/2}}. \tag{55}$$

When the bending radius becomes small, $\alpha_{\|}$ reaches different "linear asymptotes" depending on the core radius T in the range of calculations. This is mainly caused by the first and the second terms of (52). As the sign of the second term is negative, the asymptotes are below the dot–dash curve defined by α_{TM} or $\mathrm{Re}(y_{TM})/R$. We have used the term *linear asymptote*, which in an exact sense is incorrect. However, in the hollow-core diameter and bending radius which we are concerned with, some of bending loss curves are very similar to the linear curves. Therefore, we hereafter use the term *linear asymptote*. In this example, the attenuation constant $\alpha_{\|}$ of parallel polarization in waveguides with smaller core radius becomes smaller than those in waveguides with larger core radius beyond some curvature. On the other hand, $\alpha_{\perp}$ varies as $R^{-1/2}$ and there are no linear asymptotes in this range of bending radius. It is because $\mathrm{Re}(z_{TE})$ is sufficiently smaller than $\mathrm{Re}(y_{TM})$ and also the first term of (53) is dominant. Concerning a relation between theoretical and experimental bending losses for the parallel polarization, there is still a large difference. As mentioned in [15], polarization conversion from the waveguide imperfections leads to losses smaller than those predicted theoretically.

Parts (a) and (b) of Fig. 9 show attenuation constants $\alpha_{\|}$ and $\alpha_{\perp}$ in a hollow silica waveguide whose complex refractive index at 10.6 μm is $2.224 - j0.102$. In the mode with parallel polarization, the bending loss curves approach relatively similar asymptotes, whereas those of the mode with perpendicular polarization are quite different from those in a nickel waveguide and approach different linear asymptotes.

Fig. 10 shows bending losses for the germanium-coated nickel waveguide where the waveguide is designed so that $\mathrm{Re}(z_{TE}) = \mathrm{Re}(y_{TM})$ [14]; i.e., the refractive index and thickness of the germanium layer are 4.0 and 0.539 μm, respectively. In this waveguide, modes with parallel and perpendicular polarizations have the same bending loss. One should note that all asymptotes of loss curves in the waveguide are above the dot–dash curve defined by $\mathrm{Re}(y_{TM})/R$, which is different from those in nickel and silica hollow waveguides. One might still wonder why $\alpha_{\|}$ and $\alpha_{\perp}$ reach different asymptotes. This is our first finding numerically.

Finally, we add a comment why we mention the properties of the dominant mode in a bent waveguide, although the formulation itself can be applied to any mode when the convergence of the series expansion of (2) is ensured. First, when the waveguide is gently bent, only a few higher order modes are excited with a large coupling efficiency to the dominant mode. Second, for the much stronger bend than that treated in this paper, many modes are expected to have nearly the same attenuation constant as seen from the results in the general class of slab waveguides [8].

V. Conclusion

Based on the scalar equation, we have numerically evaluated electric field distributions, phase constant, and attenuation constants of the linearly polarized dominant eigenmode in bent circular hollow waveguides with arbitrary bending radii. The amounts of field shift and beam width obtained numerically are compared with those predicted by existing theories. Normalized forms of attenuation constants are presented for the parallel and perpendicular polarizations to the bending plane by using structural and material parameters. For sharply bent waveguides, useful and simple expressions are derived for the attenuation constants which are combinations of the attenuation constants of the TE and TM modes in the corresponding slab geometry with suitable weighting parameters.

Appendix I

From the following Maxwell's equations in a medium with a refractive index $n(r,\theta)$,

$$\nabla \times \tilde{H} = j\omega\epsilon_0 n^2(r,\theta)\tilde{E} \tag{A1}$$

$$\nabla \times \tilde{E} = -j\omega\mu_0 \tilde{H} \tag{A2}$$

we can deduce

$$\nabla^2\tilde{E} + k_0^2 n^2(r,\theta)\tilde{E} = -\nabla\left[\tilde{E}\cdot\nabla \ln n^2(r,\theta)\right], \tag{A3}$$

where ϵ_0, μ_0, and $k_0 = \omega(\epsilon_0\mu_0)^{1/2}$ are the dielectric constant, the permeability, and the wavenumber in free space, respectively. By employing the toroidal coordinate system in Fig. 1 and by carrying out a large number of calculations, we obtain [22]

$$\nabla_t^2 E_t + \left[k_0^2 n^2(r,\theta) - \frac{\beta^2 - \dfrac{1}{4R^2}}{\left(1 + \dfrac{r}{R}\cos\theta\right)^2}\right] E_t$$

$$= -\nabla_t\left[E_t\cdot\nabla_t \ln n^2(r,\theta)\right] - \hat{x}K \tag{A4}$$

TABLE I
VALUES OF ν AND p USED IN THE NUMERICAL CALCULATIONS TO EVALUATE EIGENVALUE AND EIGENVECTOR OF $\mathbb{M}$ FOR THE LOWEST EIGENMODE

ν	p
0	$1 \sim 9$
1	$1 \sim 8$
2	$1 \sim 7$
3	$1 \sim 6$
4	$1 \sim 5$
5	$1 \sim 4$
6	$1 \sim 3$
7	$1 \sim 3$
8	$1 \sim 2$
9	1
10	1

where the z dependence of $\exp(-j\beta z)$ is assumed and

$$\boldsymbol{E}_t = \left(1+\frac{r}{R}\cos\theta\right)^{-1/2}\tilde{\boldsymbol{E}}_t \tag{A5}$$

$$K = \frac{2}{R\left(1+\frac{r}{R}\cos\theta\right)}\left\{\nabla_t\cdot\boldsymbol{E}_t + \frac{3}{4}\left[\boldsymbol{E}_t\cdot\nabla_t \ln n^2(r,\theta)\right]\right\} \tag{A6}$$

$$\nabla_t = \hat{\boldsymbol{r}}\frac{\partial}{\partial r} + \hat{\boldsymbol{\theta}}\frac{1}{r}\frac{\partial}{\partial\theta} = \hat{\boldsymbol{x}}\frac{\partial}{\partial x} + \hat{\boldsymbol{y}}\frac{\partial}{\partial y}. \tag{A7}$$

$\tilde{\boldsymbol{E}}_t$ is the transverse component of $\tilde{\boldsymbol{E}}$, and $\hat{\boldsymbol{r}}$, $\hat{\boldsymbol{\theta}}$, $\hat{\boldsymbol{x}}$, and $\hat{\boldsymbol{y}}$ are unit vectors in the r, θ, x, and y directions, respectively. When a bending radius is sufficiently large compared with a core radius and the core radius is also sufficiently large compared with the wavelength, we have

$$\nabla_t^2\boldsymbol{E}_t + \left[k_0^2 n^2(r,\theta)\left(1+2\frac{r}{R}\cos\theta\right) - \beta^2\right]\boldsymbol{E}_t = -\nabla_t\left[\boldsymbol{E}_t\cdot\nabla_t \ln n^2(r,\theta)\right]. \tag{A8}$$

The term in the right-hand side can be neglected in a region where $n(r,\theta)$ is constant. Equation (A8) was derived by expanding

$$\left(1+\frac{r}{R}\cos\theta\right)^{-2} = 1-2\frac{r}{R}\cos\theta+3\left(\frac{r}{R}\cos\theta\right)^2+\cdots \tag{A9}$$

and neglecting terms of R^{-2} and also terms of R^{-1} which are not multiplied by β^2.

APPENDIX II

The matrix size of $\mathbb{M}$ is greatly concerned with the computer time needed; i.e., the accuracy for the eigenvalue or eigenvector and the computer time should be counterbalanced. There are two parameters, i.e., maximum numbers of ν and p, to be chosen. By doing several trials, we fix the maximum value of p so that

$$\sigma_{\nu p} + \sigma_{\nu 1} \leqq s \tag{A10}$$

where s is a parameter determining the total number of terms in a double Fourier–Bessel expansion. When b becomes large, a larger s is required to obtain sufficient accuracy for the eigenvalue and eigenvector. For b less than 100, we choose $s = 30$; therefore the total number of terms is 49. In Table I, ν and p values used in calculations are summarized.

APPENDIX III

When a waveguide is bent gently, the transverse electric field of the lowest eigenmode, i.e., the HE_{11} mode in the core region, is represented by [12]

$$E = J_0(\sigma_{01}\rho) + \frac{b}{2\sigma_{01}}(1-\rho^2)J_1(\sigma_{01}\rho)\cos\theta \tag{A11}$$

where ρ is defined by r/T. Therefore, the position x_p where E becomes maximum is determined by

$$\frac{J_1\left(\sigma_{01}\frac{x_p}{T}\right)}{J_0\left(\sigma_{01}\frac{x_p}{T}\right)} = \frac{b\sigma_{01}\frac{x_p}{T}\left[1-\left(\frac{x_p}{T}\right)^2\right]}{2\sigma_{01}^2\frac{x_p}{T}+b\left[1+\left(\frac{x_p}{T}\right)^2\right]}. \tag{A12}$$

When a waveguide is bent sharply, the transverse electric field in the core region is represented by [19]

$$E = \mathrm{Ai}\left[-(2b)^{1/3}\xi - \frac{9}{8}\pi\right]\exp\left(-\frac{1}{2}b^{1/2}\eta^2\right) \tag{A13}$$

where Ai is the Airy function; ξ is defined by $x/T - [1-(y/T)^2]^{1/2}$ and η by y/T. Therefore, x_p is expressed by

$$\frac{x_p}{T} = 1-(2b)^{-1/3}\left(a_1' + \frac{9}{8}\pi\right) \tag{A14}$$

where a_1' is equal to -1.01879 [21].

REFERENCES

[1] A. Hongo, T. Shiota, M. Suzuki, and M. Miyagi, "Germanium-coated nickel hollow waveguides for high-powered CO_2 laser light transmission," in *CLEO '88* (Anaheim, CA), Apr. 25–29, 1988, paper WL2.

[2] N. S. Kapany and J. J. Burke, *Optical Waveguides*. New York: Academic Press, 1972, pp. 18–34.

[3] M. Miyagi, "Consideration on realization of low-loss total reflection-type hollow-core fiber at mid-infrared," *Soc. Photo-Opt. Instrum. Eng.*, vol. 843, pp. 76–79, 1987.

[4] M. Miyagi and S. Kawakami, "Design theory of a dielectric-coated circular metallic waveguides for infrared transmission," *J. Lightwave Technol.*, vol. LT-2, pp. 116–126, Apr. 1984.

[5] M. Miyagi, A. Hongo, and S. Kawakami, "Transmission characteristics of dielectric-coated metallic waveguide for infrared transmission: Slab waveguide model," *IEEE J. Quantum Electron.*, vol. QE-19, pp. 136–145, Feb. 1983.

[6] T. Hidaka, T. Morikawa, and J. Shimada, "Hollow-core oxide-glass cladding optical fibers for middle-infrared region," *J. Appl. Phys.*, vol. 52, no. 7, pp. 4467–4471, July 1981.

[7] H. Krammer, "Propagation of modes in curved hollow waveguides for the infrared," *Appl. Opt.*, vol. 16, no. 8, pp. 2163–2165, Aug. 1977.

[8] M. Miyagi and S. Kawakami, "Losses and phase constant changes caused by bends in the general class of hollow waveguides for the infrared," *Appl. Opt.*, vol. 20, no. 24, pp. 4221–4226, Dec. 1981.

[9] D. Mendlovic, E. Goldenberg, S. Ruschin, J. Dror, and N. Croitoru, "Ray model for transmission of metallic-dielectric hollow bent cylindrical waveguides," *Appl. Opt.*, vol. 28, no. 4, pp. 708–712, Feb. 1989.

[10] M. E. Marhic, "Mode-coupling analysis of bending losses in IR metallic waveguides," *Appl. Opt.*, vol. 20, no. 19, pp. 3436–3441, Oct. 1981.

[11] E. A. J. Marcatili and R. A. Schmeltzer, "Hollow metallic and dielectric waveguides for long distance optical transmission and lasers," *Bell Syst. Tech. J.*, vol. 43, pp. 1783–1809, July 1964.

[12] M. Miyagi, K. Harada, and S. Kawakami, "Wave propagation and attenuation in the general class of circular hollow waveguides with uniform curvature," *IEEE Trans. Microwave Theory Tech.*, vol. MTT-32, pp. 513–531, May 1984.

[13] S. J. Wilson, R. M. Jenkins, and R. W. J. Devereux, "Hollow-core silica waveguides," *IEEE J. Quantum Electron.*, vol. QE-23, pp. 52–58, Jan. 1987.
[14] M. Miyagi, K. Harada, Y. Aizawa, and S. Kawakami, "Transmission properties of circular dielectric-coated metallic waveguides for infrared transmission," *Soc. Photo-Opt. Instrum. Eng.*, vol. 484, pp. 117–123, 1984.
[15] M. Miyagi and S. Karasawa, "Waveguide losses in sharply bent circular hollow waveguides," *Appl. Opt.*, vol. 29, no. 3, pp. 367–370, Jan. 1990.
[16] D. Marcuse, "Field deformation and loss caused by curvature of optical fibers," *J. Opt. Soc. Amer.*, vol. 66, no. 4, pp. 311–320, Apr. 1976.
[17] S. W. Lee, "Scattering by dielectric-loaded screen," *IEEE Trans. Antennas Propagat.*, vol. AP-19, pp. 656–665, Sept. 1971.
[18] S. W. Lee, W. R. Jones, and J. J. Campbell, "Convergence of numerical solutions iris-type discontinuity problems," *IEEE Trans. Microwave Theory Tech.*, vol. MTT-19, pp. 528–536, June 1971.
[19] M. E. Marhic, L. I. Kwan, and M. Epstein, "Whispering-gallery CO_2 laser," *IEEE J. Quantum Electron.*, vol. QE-15, pp. 487–490, June 1979.
[20] M. Miyagi and S. Kawakami, "Waveguide loss evaluation by the ray-optics method," *J. opt. Soc. Amer.*, vol. 73, no. 4, pp. 486–489, Apr. 1983.
[21] M. Abramowitz and I. A. Stegun, *Handbook of Mathematical Functions*. New York: Dover, 1972, p. 478.
[22] Y. Takuma, M. Miyagi, and S. Kawakami, "Eigenmode in uniformly bent circular fiber," in *1981 Tohoku-Section Joint Convention Record of Inst. Elect. Inform. Engineers Japan*, 1981, no. 1G6 (in Japanese).

✠

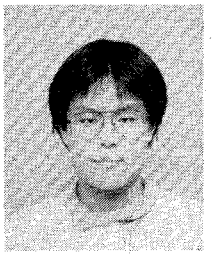

Shin-ichi Abe was born in Yamagata, Japan, on January 12, 1967. He received the B.E. degree from Tohoku University, Sendai, Japan, in 1989. He is currently working toward the M.E. degree at Tohoku University in electrical engineering. His research interests include optical hollow waveguides.

Mr. Abe is a member of the Institute of Electronics, Information, and Communication Engineers of Japan.

✠

Mitsunobu Miyagi (M'85–SM'90) was born in Hokkaido, Japan, on December 12, 1942. He graduated from Tohoku University, Sendai, Japan, in 1965 and received the M.E. and Ph.D. degrees from the same university in 1967 and 1970, respectively.

He was appointed Research Associate at the Research Institute of Electrical Communication, Tohoku University, in 1970. From 1975 to 1977, on leave from Tohoku University, he was with McGill University, Montreal, Canada, where he was engaged in research on optical communications. In 1978, he became an Associate Professor at the Research Institute of Electrical Communication. Since 1987, he has been a Professor in the Department of Electrical Communications, Faculty of Engineering, Tohoku University. He spent a month at Tianjin University, China, as a consultant to an international advisory panel dealing with the Chinese University Development Project and to the Chinese Review Commission of the Chinese Ministry of Education in 1985. His research activities cover fiber optics, the use of the aluminum anodization technique on optical devices, and guided wave technology of IR waveguides for high-powered CO_2 lasers and waveguide-type lasers. In 1989, he was awarded the Ichimura Prize for his contribution to IR hollow waveguide and its application. He has also been carrying out work on electromagnetic theory, including nonlinear wave propagation.

Dr. Miyagi is a member of the Institute of Electronics, Information, and Communication Engineers of Japan, the Optical Society of America, SPIE, and the American Institute of Physics.